THE JOURNAL OF PHYSICAL CHEMISTRY B

Article

pubs.acs.org/JPCB

The Surface Potential of the Water−Vapor Interface from Classical Simulations

Joseph R. Cendagorta and Toshiko Ichiye*

Department of Chemistry, Georgetown University, Washington, DC 20057, United States

Supporting Information

ABSTRACT: The electrochemical surface potential across the water−vapor interface provides a measure of the orientation of water molecules at the interface. However, the large discrepancies between surface potentials calculated from *ab initio* (AI) and classical molecular dynamics (MD) simulations indicate that what is being calculated may be relevant to different test probes. Although a method for extracting the electrochemical surface potential from AIMD simulations has been given, methods for MD simulations have not been clarified. Here, two methods for extracting the surface potential relevant to electrochemical measurements from MD simulations are presented. This potential is shown to be almost entirely due to the dipole contribution. In addition, the molecular origin of the dipole contribution is explored by using different potential energy functions for water. The results here show that the dipole contribution arises mainly from distortions in the hydration shell of the full hydrogen bonded waters on the liquid side of the interface, which is determined by the charge distribution of the water model. Disturbingly, the potential varies by 0.4 eV depending on the model. Although there is still no consensus on what that charge distribution should be, recent results indicate that it contains both a large quadrupole and negative charge out of the molecular plane, i.e., three-dimensional (3D) charge. Water models with 3D charge give the least distortion of the hydration shell and the best agreement with experimental surface potentials, although there is still uncertainty in the experimental values.

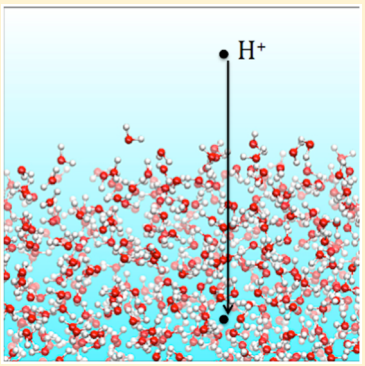

I. INTRODUCTION

Understanding the water−vapor interface plays an important role in understanding the behavior of water near surfaces and solutes.[1] Perhaps the most direct relevance is to the interface between water and hydrophobic surfaces, since hydrogen bonds are not formed at the hydrophobic surface. In addition, the surface potential across the water−vapor interface provides a measure of the orientation of the water molecules at the interface, since the water molecules must be randomly oriented deep within either the vapor or the liquid. Since the surface potential contributes to the thermodynamics of ion hydration[2−5] and to the adsorption of anions at the water−vapor interface,[6,7] understanding it has implications beyond interfacial phenomena.

Recently, a large discrepancy has been noted between "surface potentials" calculated from the electrostatic potential averaged everywhere over space using charge distributions from *ab initio* molecular dynamics (AIMD) simulations (about 3 V; for example, refs 8−10) and from classical molecular dynamics (MD) simulations (about −0.5 V; for example, refs 11 and 12). By comparison of the two, the discrepancy has been attributed to differences in the description of internal charge distribution of a water molecule as either quantum mechanical electron charge density plus nuclei or a collection of classical point charges.[13] This has led to questions about the relevance of these values to different experimental measurements.

Several authors have noted that experimental measurements of the surface potential depend on the experimental probe,[4,5,9,13] although this is still under debate[14] as is exactly what each experiment measures.[15] The average electrostatic potential calculated from an AIMD simulation has been equated to the mean inner potential measured by high-energy electron diffraction or high-energy electron holography, since the test charges are high-energy electrons that probe inside the electron density of the water molecules.[13] However, in an electrochemical experiment, the surface potential is the difference between the real free energy change upon transfer of an ion from the gas phase to the liquid phase and the chemical potential of hydration of the ion.[16−20] Since the surface potential for water is generally obtained considering this difference for a proton,[20] the test charges are protons that can probe the electrostatic potential in between the water molecules. However, the protons cannot probe inside a water molecule, since they cannot cross a second interface defined approximately by the van der Waals sphere of the water molecule. Moreover, since the electrochemical surface potential probes the orientation of water molecules at the surface and not their internal charge distribution, it probes the quantity most relevant to solvation of molecules so computer simulations can help play a role in unraveling this quantity. In addition, since modeling liquid water by classical potential energy functions

Special Issue: Branka M. Ladanyi Festschrift

Received: September 2, 2014
Revised: January 27, 2015

DOI: 10.1021/jp508878v
J. Phys. Chem. B XXXX, XXX, XXX−XXX

remains the only practical means for simulating liquid water in simulations of large macromolecules such as those found in biology, understanding the electrochemical surface potential of classical water models remains important. Thus, to calculate the surface potential for crossing the water−vapor interface relevant to electrochemistry from an AIMD simulation, the electrostatic potential was averaged only over low electron density regions, i.e., regions where a solvent molecule is not present and thus where a test charge could be.[13]

The averaged electrostatic potential can also be analyzed by expanding the electrostatic potential in a multipole expansion, resulting in an expression with terms from the dipole orientation and the traced macroscopic quadrupole.[21,22] Via this expression, a direct connection between the orientation of the dipoles of water molecules at the interface and the surface potential can be made. In addition, the differences between the AIMD and MD simulations were further localized into a term dependent on the trace of the (traced) macroscopic quadrupole tensor, with only a small contribution from the traceless quadrupole at the interface.[2] Since the trace arises from the internal charge distribution of a water molecule, it is quite different for descriptions of charge as electron density plus nuclear charge versus partial charges as in standard empirical models. Perhaps more importantly, it does not contribute to the electrochemical surface potential. However, although removing these effects is being studied for quantum mechanical charge distributions,[23] confusion still remains over how to calculate the surface potential that would be measured in an electrochemical experiment from a classical MD simulation using partial charges to describe the electrostatics.

A caveat on computer simulations is that there is no consensus on what constitutes the most essential features needed to mimic the structure and properties of liquid water. Several models of water with significantly different charge distributions are seemingly able to reproduce many bulk properties of liquid water although somewhat slight different sets of properties,[24] with supporting arguments for models with a large quadrupole and charge all in the molecular plane[25] and for models with "lone pairs" and a small quadrupole.[23,26] Recent quantum mechanical studies of a water molecule in the liquid phase provide a potential resolution in that the large quadrupole is apparently due in part to p-orbital type charge out of the molecular plane, while tetrahedral lone pairs would not contribute to the quadrupole, so that both a large quadrupole and out-of-plane charge are present.[27] More recently, a study of 13 different models, which include three-, four-, and five-site models as well as multipole models, shows that some liquid properties are affected only by the degree of tetrahedral order while others are also affected by the symmetry of the order.[28] Since symmetric strong order of the hydration shell was needed to reproduce multiple experimental properties at a given state point simultaneously, the essential features of the charge distribution of a water molecule were determined to be a large average dipole, a large quadrupole, *and* significant negative charge outside the molecular plane, which is also consistent with the quantum mechanical studies.

In addition, the effects of differences in the charge distribution of a classical water model on hydration of solutes and on water at interfaces are just beginning to be explored. For instance, in one study of the effects of the charge distribution on hydrophobic solvation, the volumetric behavior of ethanol−water mixtures as a function of ethanol concentration, which often appears in physical chemistry textbooks,[29] was explored computationally.[30] Although the observation that the partial molar volume of ethanol V_E shows a striking minimum while the partial molar volume of water V_W shows a slight peak at a mole fraction of ethanol $X_E = \sim 0.07$ has long been attributed to entropic effects in hydrophobic solvation,[31] the molecular origin has remained obscure. Recent molecular dynamics simulations show that the initial decrease in V_E is due to tighter packing of water around the hydrocarbon "tail" as the hydration shells around the tails begin to touch while the subsequant increase in V_E is due to replacement of the water hydrating the tail with loosely packing tails from other ethanols as the hydration shells break down.[30] The ability to reproduce this behavior is highly dependent on the charge distribution of the water model, which governs the behavior of the water molecules in the hydration shell around the tail. To match data from density measurements, neutron diffraction, and Raman spectroscopy of ethanol−water mixtures, the internal charge distribution of a water molecule also appears to require a large quadrupole with significant out-of-molecular plane character.

Here, surface potentials across the water−vapor interface are examined using different potential energy functions for water in MD simulations. The focus is only on the potential across the water−vapor interface and not contributions due to inhomogeneous water distributions near the cavity around a test charge in the liquid phase.[2,3,23] First, a surface potential relevant to electrochemistry is related to the mean inner potential measured by high-energy electron methods, using a multipole expansion of this equation.[21] Next, surface potentials are calculated for several nonpolarizable rigid water models with different molecular charge distributions. Finally, the molecular origins of the differences in the surface potentials, focusing on the orientation of the molecular dipoles, for the different water models are identified and discussed. These studies are leading to identification of the essential features of the charge distribution of a water molecule that give rise to the unique properties of liquid water. In addition, they are leading to understanding how these molecular properties give rise to these bulk liquid properties.

II. THEORY

The surface potential is the difference in the average electrostatic potential as a test charge is brought from deep in one phase across the interface to deep in another phase. Assuming that the water interface lies in the x and y directions, the liquid−vapor surface potential can be defined as the integral from a depth z_v in the vapor to a depth z_l in the liquid of the *macroscopic* charge density $\rho(z)$ at a distance z, where the positive z direction is toward the vapor, averaged in the x and y directions.[32,33]

$$\Delta\phi_{\text{macro}} \equiv \phi(z_l) - \phi(z_v) = -4\pi \int_{z_l}^{z_v} \mathrm{d}z \rho(z) z \tag{1}$$

The connection between this macroscopic charge density and the microscopic charge density where molecules are considered as collections of charges follows Jackson[33] (see his section 6.6; ref 33 will hence be referred to as "Jackson"). An expression similar to eq 1 can be written in terms of the spatially averaged density of microscopic charge at z, $\langle\eta(z)\rangle$,

$$\Delta\phi(z) = -4\pi \int_{z}^{z_v} \mathrm{d}z' \langle\eta(z')\rangle z' \tag{2}$$

where z_v is assumed to be deep in the vapor while z is allowed to vary so that crossing of the interface can be examined; an

DOI: 10.1021/jp508878v
J. Phys. Chem. B XXXX, XXX, XXX−XXX

electrochemical surface potential is measured at z_l deep in the liquid. In particular, when bringing a test charge in from the vapor to the liquid, if the test charge is a high-energy electron, the final point can be anywhere in the liquid including inside a water molecule, while if the test charge is a proton, the final state can only be outside any water molecule. Thus, a high-energy electron is capable of crossing two surfaces, the water–vapor interface and the van der Waals surface of a water molecule, while the proton is only capable of crossing the former.

The average density of microscopic charge $\langle\eta(z)\rangle$ is expanded in two ways here. First, it is expanded as in Jackson (see his eqs 6.87–6.90), noting that the system is inhomogeneous only along the z direction[21]

$$\langle\eta(z)\rangle = \rho(z) - \frac{\partial}{\partial z}P_z(z) + \frac{\partial^2}{\partial z^2}Q'_{zz}(z) - \ldots \tag{3}$$

where ρ is the macroscopic charge density, which is the average density of molecular charges; P_z is the z component of the macroscopic polarization, which is the average density of molecular dipoles; and Q'_{zz} is the zz component of the macroscopic quadrupole density, which is the average density of molecular quadrupoles. (Note that the spatial homogeneity in the x and y direction means that the off-diagonal elements in the quadrupole tensor must be zero because of spatial averaging, even near the interface.) For a one-component liquid,

$$\rho(\mathbf{r}) = \Big\langle \sum_{i=\text{molecules}} \delta(\mathbf{r} - \mathbf{r}_i)m^{(0)}\Big\rangle \tag{4a}$$

$$P_z(\mathbf{r}) = \Big\langle \sum_{i=\text{molecules}} \delta(\mathbf{r} - \mathbf{r}_i)m_z^{(1)}\Big\rangle \tag{4b}$$

$$Q'_{zz}(\mathbf{r}) = \frac{1}{2}\Big\langle \sum_{i=\text{molecules}} \delta(\mathbf{r} - \mathbf{r}_i)m_{zz}^{(2)}\Big\rangle \tag{4c}$$

where $\mathbf{r}_i$ is the center of the ith molecule and $\mathbf{m}^{(n)}$ is the nth moment of the charge distribution for the molecule. The first two moments are $m^{(0)} = q$, where q is the total charge of the molecule and $\mathbf{m}^{(1)} = \boldsymbol{\mu}$, where $\boldsymbol{\mu}$ is the dipole vector. The subscript z on the multipole moments indicates the component of the tensor along the z direction.

However, as discussed by Jackson (see his section 6.6), there is an apparent inconsistency between why the six components of the molecular quadrupole moment with a nonvanishing trace are needed in the macroscopic Maxwell equations while only the five independent components of the traceless molecular quadrupole moment appear in the expansion of the potential of a molecule (see chapter 4). Again following Jackson (see his eqs 6.101–6.102), when the traceless molecular quadrupole moment $\boldsymbol{\Theta} = (3\mathbf{m}^{(2)} - \text{Tr}\,\mathbf{m}^{(2)}\boldsymbol{\delta})/2$, where $\boldsymbol{\delta}$ is the Kronecker tensor (the traceless molecular multipoles are defined as in Stone)[34] and Tr denotes the trace, is substituted in our eqs 3 and 4, the terms that will give rise to traces of the higher moments can be put into $\rho(\mathbf{r})$; i.e.,

$$\langle\eta(z)\rangle = \rho(z) - \frac{\partial}{\partial z}P_z(z) + \frac{\partial^2}{\partial z^2}Q_{zz}(z) - \ldots \tag{5}$$

$$\rho(\mathbf{r}) = q\Big\langle \sum_{i=\text{molecules}} \delta(\mathbf{r} - \mathbf{r}_i)\Big\rangle + \frac{1}{6}\,\text{Tr}\,\mathbf{m}^{(2)}\frac{\partial^2}{\partial z^2}\Big\langle \sum_{i=\text{molecules}} \delta(\mathbf{r} - \mathbf{r}_i)\Big\rangle \tag{6a}$$

$$P_z(\mathbf{r}) = \Big\langle \sum_{i=\text{molecules}} \delta(\mathbf{r} - \mathbf{r}_i)\mu_z\Big\rangle \tag{6b}$$

$$Q_{zz}(\mathbf{r}) = \frac{1}{3}\Big\langle \sum_{i=\text{molecules}} \delta(\mathbf{r} - \mathbf{r}_i)\Theta_{zz}\Big\rangle \tag{6c}$$

where $\mathbf{Q}$ is the *traceless* macroscopic quadrupole tensor. This highlights the contribution of traces of the higher moments as $l = 0$ terms that are independent of rotation. Note that only the traceless terms in the higher order moments contribute to the potential seen by a test charge outside a charge distribution. Thus, since the Tr $\mathbf{m}^{(2)}$ comes outside the average in eq 6a, its contribution appears as a mean square charge radius in the macroscopic charge density (eq 6a) rather than as a contribution to the macroscopic quadrupole density (eq 6c).

In using these equations for calculating the surface potential from simulations, the multipole moments are straightforward for a simple rigid classical model but can be generalized to a polarizable, flexible model or a quantum mechanical description if they are allowed to vary with particle and position. For the quantum mechanical case, the assumption must also be made that electron density can be assigned to a molecule, which is discussed in the Supporting Information for ref 23, but this expansion can be considered a thought experiment. Since a water molecule is neutral, the first term in $\rho(\mathbf{r})$ (eqs 4a and 6a) is zero. However, to make a connection between experimental measures of the average potential and what is calculated from a classical MD simulation or an AIMD simulation, the test charge used to probe the potential in the experiment must be considered. As noted in Jackson (see his section 6.6), the microscopic electromagnetic fields vary extremely rapidly in space (and time), but since macroscopic measuring devices generally average over intervals in space (and time), spatial (but not time) averaging is necessary. In particular, the placement of the quadrupole trace term in Q'_{zz} (eq 4c) or in $\rho(\mathbf{r})$ (eq 6a) depends on the length scale being examined.

If the test charge is a high-energy electron, it can probe the region of space very near the nuclei, including the high electron density region that is normally associated with being inside the van der Waals radius of a solvent molecule. In other words, the test charge can be at points inside the van der Waals radius of a solvent molecule and so the molecular quadrupole density experienced by the test charge includes the contributions from inside the molecule in eq 4c. Thus, the spatial averaging in $\langle\eta(z)\rangle$ is described by eqs 3 and 4. When these equations are substituted into eq 2, the average potential is

$$\begin{aligned}\Delta\phi_{e^-}(z) &= -4\pi\int_z^{z_v} dz' P_z(z') - 4\pi Q'_{zz}(z) + \ldots \\ &= -4\pi\int_z^{z_v} dz' P_z(z') - 4\pi Q_{zz}(z) \\ &\quad - \frac{4\pi}{6}\rho_m(z)\,\text{Tr}\,\mathbf{m}^{(2)} + \ldots\end{aligned} \tag{7}$$

where the subscript "e^-" indicates the test charge is a high-energy electron and ρ_m is the density of a molecule (as opposed to the charge density ρ). In addition, the Q'_{zz} term and higher

DOI: 10.1021/jp508878v
J. Phys. Chem. B XXXX, XXX, XXX–XXX

order terms do not have a contribution from the vapor phase because the molecules are random deep in the vapor. The equivalence of calculating the electrostatic potential averaged over all space from a MD simulation as an integral over the charge density (eq 2) and as an expansion up to second moment terms (eq 7) (except at the interface) has been demonstrated in the literature, for instance, ref 35, and thus is shown only in the Supporting Information (Figure S1). Deep in the liquid, this becomes

$$\Delta\phi_{e^-} = -4\pi \int_{z_l}^{z_v} dz' P_z(z') - \frac{4\pi}{3} \mathrm{Tr}\, \mathbf{Q}' = -4\pi \int_{z_l}^{z_v} dz' P_z(z') - \frac{4\pi}{6}\rho_{m,l} \mathrm{Tr}\, \mathbf{m}^{(2)} \quad (8)$$

where the higher order terms disappear because the molecules are randomly oriented deep in the liquid. In the second equality, the rotational independence of the trace is used to equate $\mathrm{Tr}\,\mathbf{Q}'$ with $\rho_{m,l}\,\mathrm{Tr}\,\mathbf{m}/2$, where $\rho_{m,l}$ is the molecular density of the liquid; the equivalence in the simulations is shown in the Supporting Information (Table S1).

However, if the test charge is an ion at normal energies, it can only probe the region of space outside the van der Waals radius of a solvent molecule. In other words, the test charge never crosses the interface defined approximately by the van der Waals radius to positions in the liquid inside a water molecule. Thus, the macroscopic quadrupole moment is due only to molecular quadrupole moments outside this radius, which corresponds to the region of space where a multipole expansion of the molecular charge is valid, so the trace term due to the internal charge distribution can be put in the $\rho(\mathbf{r})$ term as in eq 6a so the spatial averaging in $\langle\eta(z)\rangle$ is described by eqs 5 and 6. When these equations are substituted into eq 2, the average potential is

$$\Delta\phi_{H^+}(z) = -\frac{4\pi}{6} \mathrm{Tr}\, \mathbf{m}^{(2)} \int_z^{z_v} dz' \rho_m''(z') z' - 4\pi \int_z^{z_v} dz' P_z(z') - 4\pi Q_{zz}(z) \approx -4\pi \int_z^{z_v} dz' P_z(z') - 4\pi Q_{zz}(z) \quad (9)$$

where the subscript "H^+" indicates the test charge is a nonbonding proton. The second derivative of the density ρ_m'' is zero deep in the vapor where the densities are constant and Q_{zz} is zero deep in the vapor where the molecules are randomly oriented, although both are nonzero at the interface. The first term has essentially no information content, and since ρ_m'' is zero deep in the liquid and nonzero only at the interface, the approximate equality is used to calculate $\Delta\phi_{H^+}$ from a simulation. Furthermore, since Q_{zz} is also zero deep in the liquid, the electrochemical surface potential from deep in the vapor to deep in the liquid is due only to the dipole polarization

$$\Delta\phi_{H^+} = -4\pi \int_{z_l}^{z_v} dz P_z(z) \quad (10)$$

The difficulty comes when trying to calculate these quantities from simulations. To calculate the surface potential seen by a high-energy electron $\Delta\phi_{e^-}$, the most straightforward calculation is to use eq 2, i.e., averaging the charge density over all space in an AIMD simulation as is generally done. Of course, it does not make sense to calculate $\Delta\phi_{e^-}$ from a classical MD simulation. However, $\Delta\phi_{H^+}$ is somewhat more problematic. As mentioned earlier, $\Delta\phi_{H^+}$ has been calculated from an AIMD simulation by including only regions of space into the average where the electron density is low.[13] Alternatively, one could combine eqs 2, 7, and 9

$$\Delta\phi_{H^+}(z) \approx -4\pi \int_z^{z_v} dz' \langle\eta(z')\rangle z' + \frac{4\pi}{6}\rho_m(z)\,\mathrm{Tr}\,\mathbf{m}^{(2)} \quad (11)$$

As above, the contribution of the last term is very small except at the interface, while the contribution of the second term appears even in the liquid phase. Thus, from deep in the vapor to deep in the liquid

$$\Delta\phi_{H^+} = -4\pi \int_z^{z_v} dz' \langle\eta(z')\rangle z' + \frac{4\pi}{6}\rho_{m,l}\,\mathrm{Tr}\,\mathbf{m}^{(2)} \quad (12)$$

The second moment for a molecule in the liquid phase appears in eq 12, which requires a prescription for partitioning electron density between molecules.[36,37] In earlier works, $\Delta\phi_{H^+}$ has generally been calculated from classical MD simulations by either eq 2 or eq 8; instead, either eq 9 should be used where Q_{zz} must be traceless, or equivalently eq 11 can be used to remove the contribution of the trace from eq 2.

Thus, the crux of the difference between a high-energy electron versus a proton as the test charge is whether the $\mathrm{Tr}\,\mathbf{m}^{(2)}$ term belongs in the macroscopic charge density or in the macroscopic quadrupole density. In eqs 3 and 4, it is put in the quadrupole term because the charges of the molecules making up the liquid, whether partial charges or nuclear and electronic, are viewed as a sea of charges. This is appropriate when the test charges are high-energy electrons. In this view, the macroscopic quadrupole density includes variations of the microscopic field due to the internal charge distribution. However, in eqs 5 and 6, the $\mathrm{Tr}\,\mathbf{m}^{(2)}$ term is put into the average charge density, where it defines the mean square charge density (see explanatory text for eq 6.102, Jackson). This is appropriate when the test charges are protons, which cannot probe inside the molecules comprising the liquid. In this role, it depends on $\partial^2\rho/\partial z^2$, which disappears deep in the liquid and vapor.

Furthermore, it should be noted that the trace contribution is not meaningful for a classical potential using only partial charges, since it does not reflect the internal charge distribution of a real water molecule, although using a Gaussian negative charge density may be more reasonable, nor does it contribute to intermolecular interactions, including with a test charge. Since the trace is independent of rotation, the contribution of trace terms to the average electrostatic potential is very large and positive (+3 to 4 eV) for the AIMD results. For partial charge potentials, the contribution of trace terms is very large but *negative* (−0.25 to −0.9 eV, see the Supporting Information) and thus gives large errors in the values from simulation if its contribution is not removed.

III. SIMULATION METHODS

The molecular dynamics simulations were performed with the molecular mechanics package CHARMM[38] version c36 using the SPC/E,[39] TIP3P,[40] TIP4P,[40] TIP4P-Ew,[41] TIP5P-0.5,[42] TIP5P-E,[43] SSDQO1,[44] and SSDQO2 parameters for waters. The results for SPC/E, TIP4P, TIP5P-0.5, and SSDQO2 appear in the Supporting Information; the latter two are explained more fully there. The soft sticky dipole−quadrupole−octupole (SSDQO) water model[45] was incorporated into CHARMM using MSCALE.[46] The electrostatic interactions

DOI: 10.1021/jp508878v
J. Phys. Chem. B XXXX, XXX, XXX−XXX

were calculated via the particle mesh Ewald[47] (PME) method with a β-spline coefficient equal to 6 and a κ value of 0.34 Å^{-1}. The SHAKE[48] algorithm was used to constrain covalent bonds involving hydrogen atoms. All simulations employed the leapfrog Verlet[49] algorithm with a time step of 1 fs.

The simulations were carried out in the *NVT* ensemble with a target temperature of 298 K using the Nosé−Hoover algorithm.[50,51] For the initial box of 216 water molecules, velocities were assigned to the entire system according to a Gaussian distribution every 200 fs for 50 ps and then scaled every 1 ps if the temperature exceeded 298 ± 5 K for 250 ps. The box was then equilibrated undisturbed for another 700 ps. A 2 × 2 expansion in the x and y directions of the equilibrated cube was then performed in order to create a slab of 864 water molecules. The cubic box length was ∼38 Å, and periodic boundary conditions were employed resulting in vapor/water/vapor layers in the z-direction of lengths 9.5/19/9.5 Å, respectively. These boxes were allowed to run unperturbed for 4 ns with the last 2 ns used for analysis.

The surface interface was defined as the point where the water density nears 50%. The "liquid" and "vapor" sides of the interface were defined as 3 Å in the respective directions, corresponding to approximately one monolayer of water. All values were averaged across both sides of the slab. The spacing in the z-direction for analysis was 0.25 Å.

IV. RESULTS AND DISCUSSION

The electrochemically measured contribution to the surface potential $\Delta\phi_{H^+}$ as a function of z is calculated using eqs 9 and 11 for different nonpolarizable rigid models of water (Figure 1).

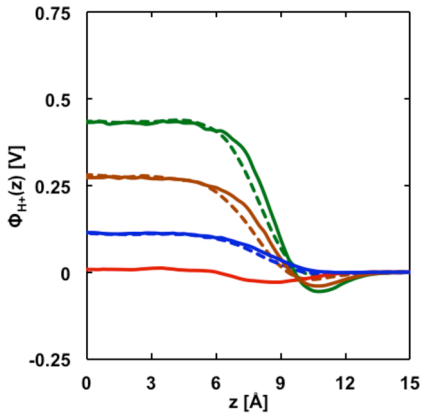

Figure 1. Surface potential ϕ_{H^+} calculated from eq 7 (dotted line), which is mainly the dipole contribution, and from eq 9 (solid line), which contains other contributions at the interface, for the various water models: TIP3P (brown), TIP4P-Ew (green), TIP5P-E (blue), and SSDQO1 (red) as a function of distance z from the center of the water slab.

The contribution of the traceless quadrupole **Q** in eq 9 was small even at the interface so the differences between eqs 9 and 11 at the interface are due to the trace term, which disappears deep in the liquid. As noted in section III, the contribution of the trace term of a partial charge model has no physical relevance, and since it is quite large and negative for 3- and 4-point models (−0.8 to −0.9 eV), the correct values of $\Delta\phi_{H^+}(z)$ are opposite in sign from what is normally reported. It is also noted that single-site, molecular multipole models such as the SSDQO models use traceless multipoles in the interaction energies, so that the macroscopic second moment trace is zero. On the other hand, the trace contribution is much smaller for 5-point models and nonexistent for point multipole models, so although they also change sign for the 5-point models, the error is much smaller.

The dipole contribution to $\Delta\phi_{H^+}(z_l)$ is a measure of the orientation of the water molecules at the interface, where the interface is defined as the distance where the density reaches 50% of the bulk value (at ∼9 Å from the center of the liquid slab for these simulations). In general, the dipole contribution to $\Delta\phi_{H^+}(z_l)$ becomes slightly negative first, indicating the hydrogens pointing away from the surface, and then positive, indicating the hydrogens pointing toward the surface, as the surface is approached from the vapor phase (Figure 1). In addition, the integrand of the dipole contribution as a function of distance (Figure 2, solid) can be separated into contributions from water molecules that have four nearest neighbors (Figure 2, dashed) and three or less nearest neighbors (Figure 2, dotted). The water molecules on the vapor side of the interface have mostly three or few neighbors and have a slight tendency to point away from the liquid. On the other hand, the water molecules on the liquid side of the interface tend to have their hydrogens pointing toward the liquid phase, regardless of the number of neighbors, indicating a tendency for the formation of hydrogen bonds between their hydrogens and oxygens of the liquid.

Furthermore, the different models of water studied here have large differences in the dipole orientation, which give rise to a large range (between 0.01 and 0.4 eV) for surface potentials of the models (Figure 2, results are shown for representative models, while other models are in the Supporting Information). Moreover, the differences appear characteristic of whether the model is two-dimensional (2D) with three (TIP3P) or four (TIP4P-Ew) partial charge sites and no out-of-plane (i.e., 2D) charge, which have large surface potentials (Figure 2a,b), or is three-dimensional (3D) with five sites (TIP5P-E) or multipoles (SSDQO1) and out-of-plane (i.e., 3D) character, which have small surface potentials (Figure 2c,d). Interestingly, the differences lie mainly in the interfacial water molecules on the liquid side of the interface that have four molecules in their hydration shell (Figure 2, dashed).

Since the coordination number of pure liquid water is about 4.3 according to diffraction studies,[52] bulk liquid is thought to be composed mostly of water with four neighbors (two hydrogen bond donors and two hydrogen bond acceptors) and water with five neighbors, which indicates at least one of the neighbors is weakly hydrogen bonded, since a water molecule can participate in a maximum of four strong hydrogen bonds. In addition, the degree of tetrahedral order of the neighbors along the hydrogen directions and the lone pair directions is an indication of hydrogen bond strength, since the greater the order, the more linear a hydrogen bond tends to be, although the O···H−O angle or hydrogen bond energies are better indicators. Examining the percentage of water molecules as the interface is approached from the liquid side (Figure 3, results are shown for representative models, while other models in the Supporting Information), all of the models show a decrease in the number of waters with five neighbors as expected. Concurrent with this decrease, the 2D models show a slight but noticeable increase in the water molecules with four neighbors as well as those with three or fewer (Figure 3a,b), while the 3D models show little increase in molecules with four neighbors and instead show an increase mostly in those with

DOI: 10.1021/jp508878v
J. Phys. Chem. B XXXX, XXX, XXX−XXX

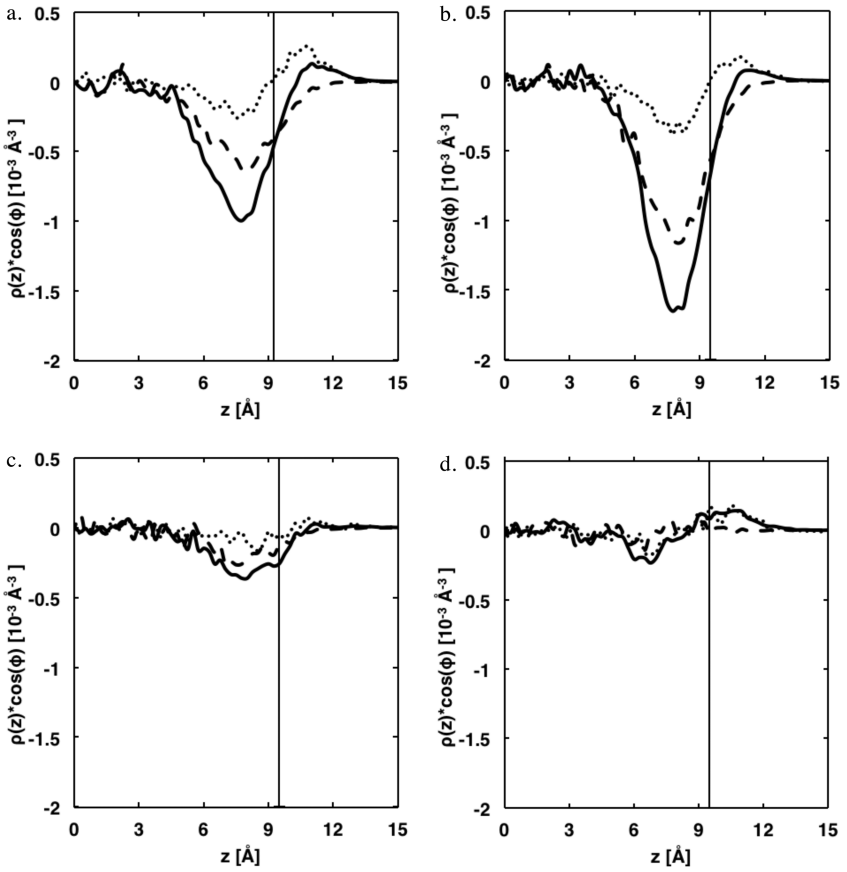

Figure 2. Density weighted dipole polarization of all waters (solid), waters with three or less (dotted) and four (dashed) neighbors as a function of distance z from the center of the water slab. (a) TIP3P, (b) TIP4P-E, (c) TIP5P-E, (d) SSDQO1. The angle ϕ is between the dipole vector and the surface normal. The distance at which the density reaches 50% of the bulk value is indicated by a solid vertical line.

three or fewer neighbors (Figure 3c,d). This difference leads to the different dipolar contribution. In the 2D models, the preference for accepting weak distorted hydrogen bonds apparently favors the orientation of the dipole pointing toward the liquid, since strong bonds can be donated to the liquid while weak distorted hydrogen bonds can be accepted from the vapor side interfacial water molecules (Figure 4, left), while in the 3D models, there is a tendency to break the hydrogen bonds from the vapor side water rather than form distorted bonds (Figure 4, right). For both types of models, the molecules with their dipoles pointing toward the vapor tend to break hydrogen bonds with neighbors on the vapor side, since they donate only to a more restricted angular range of neighbors (Figure 4, center). The net result is a stronger dipole contribution from the 2D models, since they are more strongly ordered hydrogen bond donors and more disordered hydrogen bond acceptors, while 3D models are more symmetric in their hydrogen bond capabilities as either donors or acceptors so neither orientation of the dipole is favored as strongly.

The $\Delta\phi_{H^+}$ obtained from simulations with 3D models are small (0.01−0.1 eV), which is more consistent with those from experiment (0.03[17]−0.14[20] eV). Also, the 3D models do not show a significant increase in distorted hydrogen bonds in fully hydrated water molecules at the interface but instead have more broken hydrogen bonds, which is consistent with surface vibrational spectroscopic experiments of the water−vapor interface that also indicate water molecules at the interface have either strong or broken hydrogen bonds,[53] although water apparently exhibits weak hydrogen bonds at interfaces with hydrophobic liquids.[54] More quantitative enumeration of strong and broken bonds by surface vibration experiments may help resolve some of these issues. In addition, other computational studies show that the 3D models have very tetrahedral hydrogen bonds around the hydrophobic tail of ethanol and exhibit the minimum in the partial molar volume of ethanol in ethanol−water mixtures, which is consistent with experiment, while 2D models have distorted hydrogen bonds and do not exhibit the minimum.[30]

V. CONCLUSIONS

The electrochemically measured surface potential, defined as the averaged electrostatic potential felt by a proton as it crosses the water−vapor interface,[20] only probes the area outside of a solvent (water) molecule defined approximately by its van der Waals sphere. Thus, the contributions from the trace of the second moment, which is large compared to the dipole contribution, must be removed from electrostatic potentials obtained from integrating charge over all space in classical (or *ab initio*) MD simulations, or alternatively by just averaging over the dipole polarization in the simulations, to be relevant to electrochemical measurements. The results here also show that the surface potential contains only contributions from dipole orientation deep in the liquid, although a small contribution from higher traceless multipoles appears at the interface, which supports the general interpretation of the electrochemical surface potential as a measure of the orientation of the water dipoles at the surface.[18] Thus, when properly extracted from the simulation, comparison between the surface potentials from

DOI: 10.1021/jp508878v
J. Phys. Chem. B XXXX, XXX, XXX−XXX

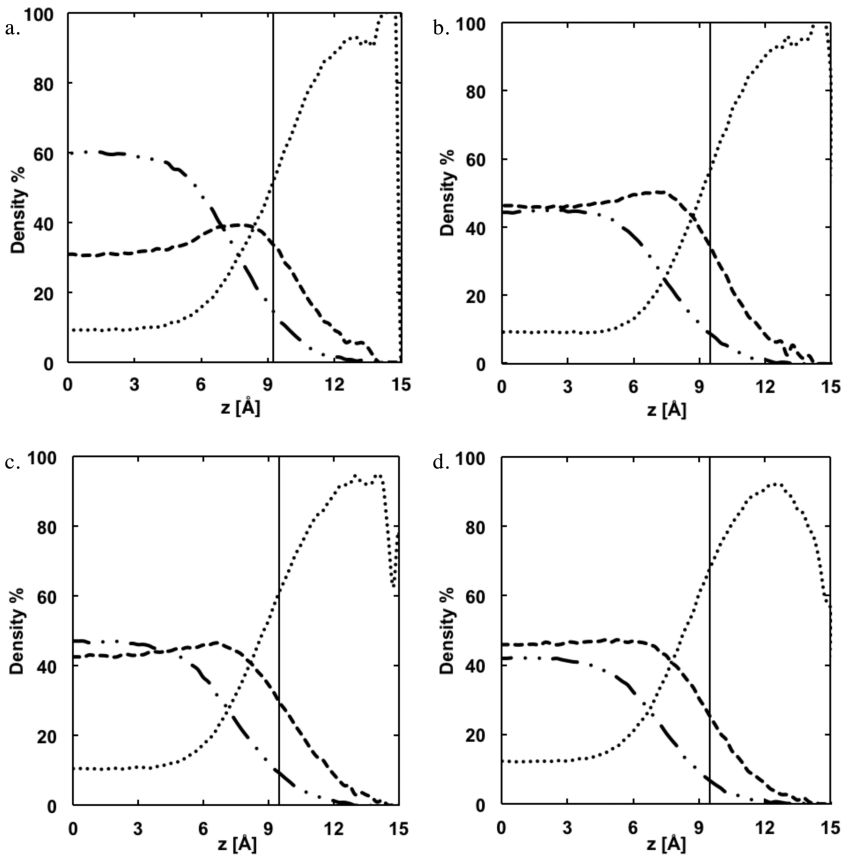

Figure 3. Percent of water molecules with one to three (dotted), four (dashed), and five (dot-dashed) neighbors as a function of distance z from the center of the water slab. (a) TIP3P, (b) TIP4P-E, (c) TIP5P-E, (d) SSDQO1. The distance at which the density reaches 50% of the bulk value is indicated by a solid vertical line.

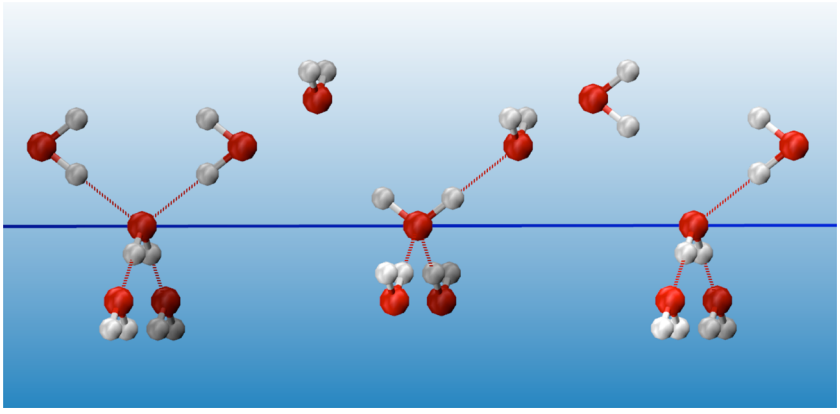

Figure 4. Schematic of water molecules and their first hydration shell at the interface (blue line), with vapor at the top and liquid at the bottom. Left, 2D model with hydrogens pointing toward the liquid; center, 2D or 3D models with hydrogens pointing toward the vapor; right, 3D models with hydrogens pointing toward the liquid.

simulation and experiment is a good test of how well classical force fields reproduce the orientation. However, while the contribution of the trace in an AIMD simulation is reflective of the internal charge distribution of a water molecule, the contribution of the trace in a MD simulation using partial charge electrostatics is meaningless, since their internal charge distributions are not parametrized to reproduce electrostatic potentials inside the van der Waals radius.

Furthermore, examination of different water models shows that different internal charge distributions give rise to large differences (~0.4 eV) in the surface potential. These differences are due to the dipole orientation at the interface, indicating that the interfacial structure is significantly different. Comparisons with experimental measurement of the electrochemical surface potential and surface vibrational spectroscopy of water−vapor interfaces indicate that, in nonpolarizable rigid water models, those with 3D charge distributions are more consistent with experiment, although there is still uncertainty in the electrochemical measurements.

DOI: 10.1021/jp508878v
J. Phys. Chem. B XXXX, XXX, XXX−XXX

■ ASSOCIATED CONTENT

Supporting Information

Four supporting figures are provided. Figure S1 compares electrostatic potential calculated using eqs 2 and 7. Figures S2, S3, and S4 are the surface potential ϕ_{H^+} calculated from eq 9 and from eq 11 similar to Figure 1, the density weighted dipole polarization as a function of distance similar to Figure 2, and the percent of water molecules similar to Figure 3, respectively, but for SPC/E, TIP4P, TIP5P-0.5, and SSDQO2. More detailed explanations of TIP5P-0.5 and SSDQO2 are also given. Finally, a table comparing $\mathrm{Tr}\,\mathbf{Q}'$ with $\rho_l \mathrm{Tr}\,\mathbf{m}/2$ for different models from the simulations is given. This material is available free of charge via the Internet at http://pubs.acs.org.

■ AUTHOR INFORMATION

Corresponding Author

*E-mail: ti9@georgetown.edu.

Notes

The authors declare no competing financial interest.

■ ACKNOWLEDGMENTS

The authors are grateful for support from the National Science Foundation through Grant No. CHE-1158267 and from the McGowan Foundation. This work used the Extreme Science and Engineering Discovery Environment (XSEDE), which is supported by National Science Foundation grant number OCI-1053575; the Lobos cluster at the Laboratory for Computational Biology, National Heart, Lung, and Blood Institute, National Institutes of Health, through the generosity of Bernard R. Brooks; and the Matrix and Medusa clusters, maintained by University Information Services at Georgetown University.

■ REFERENCES

(1) Wilson, M. A.; Pohorille, A.; Pratt, L. R. Surface Potential of the Water Liquid−Vapor Interface. *J. Chem. Phys.* **1988**, *88*, 3281−3285.

(2) Beck, T. L. The Influence of Water Interfacial Potentials on Ion Hydration in Bulk Water and near Interfaces. *Chem. Phys. Lett.* **2013**, *561*−*562*, 1−13.

(3) Pollard, T.; Beck, T. L. Quasichemical Analysis of the Cluster-Pair Approximation for the Thermodynamics of Pair Hydration. *J. Chem. Phys.* **2014**, *140*, 224507.

(4) Hünenberger, P. H.; Reif, M. M. *Single-Ion Solvation. Experimental and Theoretical Approaches to Elusive Thermodynamic Quantities.*; Royal Society of Chemistry: London, 2011.

(5) Reif, M. M.; Hünenberger, P. H. Computation of Methodology-Independent Single-Ion Solvation Properties from Molecular Simulations. III. Correction Terms for the Solvation Free Energies, Enthalpies, Entropies, Heat Capacities, Volumes, Compressibilities and Expansivities of Solvated Ions. *J. Chem. Phys.* **2011**, *134*, 144103.

(6) Baer, M. D.; Stern, A. C.; Levin, Y.; Tobias, D. J.; Mundy, C. J. Electrochemical Surface Potential Due to Classical Point Charge Models Drives Anion Adsorption to the Air-Water Interface. *J. Phys. Chem. Lett.* **2014**, *3*, 1565−1570.

(7) Stern, A. C.; Baer, M. D.; Mundy, C. J.; Tobias, D. J. Thermodynamics of Iodide Adsorption at the Instantaneous Air-Water Interface. *J. Chem. Phys.* **2013**, *38*, 114709.

(8) Kathmann, S. M.; Kuo, I. F. W.; Mundy, C. J. Electronic Effects on the Surface Potential at the Vapor−Liquid Interface of Water. *J. Am. Chem. Soc.* **2009**, *131*, 17522−17522.

(9) Leung, K. Surface Potential at the Air−Water Interface Computed Using Density Functional Theory. *J. Phys. Chem. Lett.* **2009**, *1*, 496−499.

(10) Vorobyov, I.; Allen, T. W. The Electrostatics of Solvent and Membrane Interfaces and the Role of Electronic Polarizability. *J. Chem. Phys.* **2010**, *132*, 185101.

(11) Dang, L. X.; Chang, T.-M. Molecular Dynamics Study of Water Clusters, Liquid, and Liquid−Vapor Interface of Water with Many-Body Potentials. *J. Chem. Phys.* **1997**, *106*, 8149−8159.

(12) Feller, S. E.; Pastor, R. W.; Rojnuckarin, A.; Bogusz, S.; Brooks, B. R. Effect of Electrostatic Force Trunction on Interfacial and Transport Properties of Water. *J. Phys. Chem.* **1996**, *100*, 17011−17020.

(13) Kathmann, S. M.; Kuo, I. F. W.; Mundy, C. J.; Schenter, G. K. Understanding the Surface Potential of Water. *J. Phys. Chem. B* **2011**, *115*, 4369−4377.

(14) You, X.; Chaudhari, M. I.; Pratt, L. R. Xxi. Comparison of Mechanical and Thermodynamical Evaluations of Electrostatic Potential Differences between Electrolyte Solutions. In *Aqua Incognito: Why Ice Floats and Galileo 400 Years On*; Nostro, P. L., Ninham, B. W., Eds.; Connor Court: Ballarat, Australia, 2014; pp 434−442.

(15) Pethica, B. A. Are Electrostatic Potentials between Regions of Different Chemical Composition Measurable? The Gibbs-Guggenheim Principle Reconsidered, Extended and Its Consequences Revisited. *Phys. Chem. Chem. Phys.* **2007**, *9*, 6253−6262.

(16) Randles, J. E. B. The Real Hydration Energies of Ions. *Trans. Faraday Soc.* **1956**, *52*, 1573−1581.

(17) Farrell, J. R.; McTigue, P. Precise Compensating Potential Difference Measurements with a Voltaic Cell: The Surface Potential of Water. *J. Electroanal. Chem. Interfacial Electrochem.* **1982**, *139*, 37−56.

(18) Trasatti, S. The Absolute Electrode Potential: An Explanatory Note. *Pure Appl. Chem.* **1986**, *58*, 955−966.

(19) Trasatti, S. Interfacial Behaviour of Non-Aqueous Solvents. *Electrochim. Acta* **1987**, *32*, 843−850.

(20) Fawcett, W. R. The Ionic Work Function and Its Role in Estimating Absolute Electrode Potentials. *Langmuir* **2008**, *24*, 9868−9875.

(21) Wilson, M. A.; Pohorille, A.; Pratt, L. R. Comment on "Study on the Liquid−Vapor Interface of Water. I. Simulation Results of Thermodynamic Properties and Orientational Structure". *J. Chem. Phys.* **1989**, *90*, 5211−5213.

(22) Pratt, L. R. Contact Potentials of Solution Interfaces: Phase Equilibrium and Interfacial Electric Fields. *J. Phys. Chem.* **1992**, *96*, 25−33.

(23) Remsing, R. C.; Baer, M. D.; Schenter, G. K.; Mundy, C. J.; Weeks, J. D. The Role of Broken Symmetry in Solvation of a Spherical Cavity in Classical and Quantum Water Models. *J. Phys. Chem. Lett.* **2014**, *5*, 2767−2774.

(24) Vega, C.; Abascal, J. L. F. Simulating Water with Rigid Non-Polarizable Models: A General Perspective. *Phys. Chem. Chem. Phys.* **2011**, *13*, 19663−19688.

(25) Abascal, J. L. F.; Vega, C. The Water Forcefield: Importance of Dipolar and Quadrupolar Interactions. *J. Phys. Chem. C* **2007**, *111*, 15811−15822.

(26) Fernandez, M. V.; Artacho, E. Electrons and Hydrogen-Bonded Connectivity in Liquid Water. *Phys. Rev. Lett.* **2006**, *96*, 016404.

(27) Niu, S.; Tan, M.-L.; Ichiye, T. The Large Quadrupole of Water Molecules. *J. Chem. Phys.* **2011**, *134*, 134501.

(28) Tan, M.-L.; Cendagorta, J. R.; Ichiye, T. The Molecular Charge Distribution, the Hydration Shell, and the Unique Properties of Liquid Water. *J. Chem. Phys.* **2014**, *141*, 244504.

(29) Atkins, P.; de Paula, J. *Physical Chemistry*; W. H. Freeman: New York, 2006; Vol. *1*. Thermodynamics and Kinetics.

(30) Tan, M.-L.; Cendagorta, J. R.; Ichiye, T. Effects of Micro-complexity on Hydrophobic Hydration in Amphiphiles. *J. Am. Chem. Soc.* **2013**, *135*, 4918−4921.

(31) Frank, H. S.; Evans, M. W. Free Volume and Entropy in Condensed Systems. Iii. Entropy in Binary Liquid Mixtures; Partial Molal Entropy in Dilute Solutions; Structure and Thermodynamics in Aqueous Electrolytes. *J. Chem. Phys.* **1945**, *13*, 507−532.

(32) Landau, L. D.; Lifshitz, E. M.; Pitaevskii, L. P. *Electrodynamics of Continuous Media*, 2nd ed.; Pergamon Press: Oxford, U.K., 1984.

(33) Jackson, J. D. *Classical Electrodynamics*, 3rd ed.; Wiley: New York, 1975.

DOI: 10.1021/jp508878v
J. Phys. Chem. B XXXX, XXX, XXX−XXX

(34) Stone, A. J. *The Theory of Intermolecular Forces*; Clarendon: Oxford, U.K., 1996.
(35) Warren, G. L.; Patel, S. Hydration Free Energies of Monovalent Ions in Transferable Intermolecular Potential Four Point Fluctuating Charge Water: An Assessment of Simulation Methodology and Force Field Performance and Transferability. *J. Chem. Phys.* **2007**, *127*, No. 064509.
(36) Silvestrelli, P. L.; Parrinello, M. Structural, Electronic, and Bonding Properties of Liquid Water from First Principles. *J. Chem. Phys.* **1999**, *111*, 3572−3580.
(37) Delle Site, L.; Alavi, A.; Lynden-Bell, R. M. The Electrostatic Properties of Water Molecules in Condensed Phases: An *Ab Initio* Study. *Mol. Phys.* **1999**, *96*, 1683−1693.
(38) Brooks, B. R.; Brooks, C. L., III; MacKerell, A. D., Jr.; Nilsson, L.; Petrella, R. J.; Roux, B.; Won, Y.; Archontis, G.; Bartels, C.; Boresch, S.; et al. Charmm: The Biomolecular Simulation Program. *J. Comput. Chem.* **2009**, *30*, 1545−1614.
(39) Berendsen, H. J. C.; Grigera, J. R.; Straatsma, T. P. The Missing Term in Effective Pair Potentials. *J. Phys. Chem.* **1987**, *91*, 6269−6271.
(40) Jorgensen, W. L.; Chandrasekhar, J.; Madura, J. D.; Impey, R. W.; Klein, M. L. Comparison of Simple Potential Functions for Simulating Liquid Water. *J. Chem. Phys.* **1983**, *79*, 926−935.
(41) Horn, H. W.; Swope, W. C.; Pitera, J. W.; Madura, J. D.; Dick, T. J.; Hura, G. L.; Head-Gordon, T. Development of an Improved Four-Site Water Model for Biomolecular Simulations: Tip4p-Ew. *J. Chem. Phys.* **2004**, *120*, 9665−9678.
(42) Mahoney, M. W.; Jorgensen, W. L. A Five-Site Model for Liquid Water and the Reproduction of the Density Anomaly by Rigid, Nonpolarizable Potential Functions. *J. Chem. Phys.* **2000**, *112*, 8910−8922.
(43) Rick, S. W. A Reoptimization of the Five-Site Water Potential (Tip5p) for Use with Ewald Sums. *J. Chem. Phys.* **2004**, *2004*, 6085−6093.
(44) Te, J. A.; Ichiye, T. Temperature and Pressure Dependence of the Optimized Soft Sticky Dipole-Quadrupole-Octupole Water Model. *J. Chem. Phys.* **2010**, *132*, 114511.
(45) Ichiye, T.; Tan, M.-L. Soft Sticky Dipole-Quadrupole-Octupole Potential Energy Function for Liquid Model: An Approximate Moment Expansion. *J. Chem. Phys.* **2006**, *124*, 134504.
(46) Woodcock, H. L.; Miller, B. T.; Hodoscek, M.; Okur, A.; Larkin, J. D.; Ponder, J. W.; Brooks, B. R. Mscale: A General Utility for Multiscale Modeling. *J. Chem. Theory Comput.* **2011**, *7*, 1208−1219.
(47) Darden, T. A.; York, D. M.; Pedersen, L. G. Particle Mesh Ewald: An Nlog(N) Method for Ewald Sums in Large Systems. *J. Chem. Phys.* **1993**, *98*, 10089−10092.
(48) Rychaert, J. P.; Ciccotti, G.; Berendsen, H. J. C. Numerical Integration of the Cartesian Equation of Motion of a System with Constraints: Molecular Dynamics of N-Alkanes. *J. Comput. Phys.* **1977**, *23*, 327−341.
(49) Verlet, L. Computer "Experiments" On Classical Fluids. Ii. Equilibrium Correlation Functions. *Phys. Rev.* **1968**, *165*, 201−214.
(50) Nosé, S. A Unified Formulation of the Constant Temperature Molecular Dynamics Methods. *J. Chem. Phys.* **1984**, *81*, 511−519.
(51) Hoover, W. G. Canonical Dynamics: Equilibrium Phase-Space Distributions. *Phys. Rev. A* **1985**, *31*, 1695−1697.
(52) Soper, A. K. The Radial Distribution Functions of Water and Ice from 220 to 673 K and at Pressures up to 400 MPa. *Chem. Phys.* **2000**, *258*, 121−137.
(53) Du, Q.; Freysz, E.; Shen, Y. R. Surface Vibrational Spectroscopic Studies of Hydrogen Bonding and Hydrophobicity. *Science* **1994**, *264*, 826−828.
(54) Scatena, L. F.; Brown, M. G.; Richmond, G. L. Water at Hydrophobic Surfaces: Weak Hydrogen Bonding and Strong Orientation Effects. *Science* **2001**, *292*, 908−912.

DOI: 10.1021/jp508878v
J. Phys. Chem. B XXXX, XXX, XXX−XXX